

AFRL-PR-WP-TP-2006-263

**NEAR-INFRARED DIODE LASER
ABSORPTION DIAGNOSTIC FOR
TEMPERATURE AND WATER
VAPOR IN A SCRAMJET
COMBUSTOR (POSTPRINT)**



**Jonathan T. C. Liu, Gregory B. Rieker, Jay B. Jeffries, Mark R. Gruber,
Campbell D. Carter, Tarun Mathur, and Ronald K. Hanson**

NOVEMBER 2005

Approved for public release; distribution is unlimited.

STINFO COPY

© 2005 Optical Society of America

**The U.S. Government is joint author of the work and has the right to use, modify,
reproduce, release, perform, display, or disclose the work.**

**PROPULSION DIRECTORATE
AIR FORCE MATERIEL COMMAND
AIR FORCE RESEARCH LABORATORY
WRIGHT-PATTERSON AIR FORCE BASE, OH 45433-7251**

REPORT DOCUMENTATION PAGE				<i>Form Approved</i> OMB No. 0704-0188											
<p>The public reporting burden for this collection of information is estimated to average 1 hour per response, including the time for reviewing instructions, searching existing data sources, gathering and maintaining the data needed, and completing and reviewing the collection of information. Send comments regarding this burden estimate or any other aspect of this collection of information, including suggestions for reducing this burden, to Department of Defense, Washington Headquarters Services, Directorate for Information Operations and Reports (0704-0188), 1215 Jefferson Davis Highway, Suite 1204, Arlington, VA 22202-4302. Respondents should be aware that notwithstanding any other provision of law, no person shall be subject to any penalty for failing to comply with a collection of information if it does not display a currently valid OMB control number. PLEASE DO NOT RETURN YOUR FORM TO THE ABOVE ADDRESS.</p>															
1. REPORT DATE (DD-MM-YY) November 2005		2. REPORT TYPE Journal Article Postprint		3. DATES COVERED (From - To) 09/01/2004 – 12/31/2004											
4. TITLE AND SUBTITLE NEAR-INFRARED DIODE LASER ABSORPTION DIAGNOSTIC FOR TEMPERATURE AND WATER VAPOR IN A SCRAMJET COMBUSTOR (POSTPRINT)				5a. CONTRACT NUMBER In-house											
				5b. GRANT NUMBER											
				5c. PROGRAM ELEMENT NUMBER 62203F											
6. AUTHOR(S) Jonathan T. C. Liu, Gregory B. Rieker, Jay B. Jeffries, and Ronald K. Hanson (Stanford University) Mark R. Gruber and Campbell D. Carter (AFRL/PRAS) Tarun Mathur (Innovative Scientific Solutions, Inc.)				5d. PROJECT NUMBER 3012											
				5e. TASK NUMBER AI											
				5f. WORK UNIT NUMBER 00											
7. PERFORMING ORGANIZATION NAME(S) AND ADDRESS(ES) Stanford University High Temperature Gasdynamics Laboratory Department of Mechanical Engineering Stanford, CA 94305				8. PERFORMING ORGANIZATION REPORT NUMBER AFRL-PR-WP-TP-2006-263											
<table border="0" style="width: 100%;"> <tr> <td style="width: 33%;">Propulsion Sciences Branch (AFRL/PRAS)</td> <td style="width: 33%;">Innovative Scientific Solutions, Inc.</td> </tr> <tr> <td>Aerospace Propulsion Division</td> <td>Dayton, OH 45440</td> </tr> <tr> <td>Propulsion Directorate</td> <td></td> </tr> <tr> <td>Air Force Research Laboratory</td> <td></td> </tr> <tr> <td>Air Force Materiel Command</td> <td></td> </tr> <tr> <td>Wright-Patterson AFB, OH 45433-7251</td> <td></td> </tr> </table>						Propulsion Sciences Branch (AFRL/PRAS)	Innovative Scientific Solutions, Inc.	Aerospace Propulsion Division	Dayton, OH 45440	Propulsion Directorate		Air Force Research Laboratory		Air Force Materiel Command	
Propulsion Sciences Branch (AFRL/PRAS)	Innovative Scientific Solutions, Inc.														
Aerospace Propulsion Division	Dayton, OH 45440														
Propulsion Directorate															
Air Force Research Laboratory															
Air Force Materiel Command															
Wright-Patterson AFB, OH 45433-7251															
9. SPONSORING/MONITORING AGENCY NAME(S) AND ADDRESS(ES) Propulsion Directorate Air Force Research Laboratory Air Force Materiel Command Wright-Patterson AFB, OH 45433-7251				10. SPONSORING/MONITORING AGENCY ACRONYM(S) AFRL-PR-WP											
				11. SPONSORING/MONITORING AGENCY REPORT NUMBER(S) AFRL-PR-WP-TP-2006-263											
12. DISTRIBUTION/AVAILABILITY STATEMENT Approved for public release; distribution is unlimited.															
13. SUPPLEMENTARY NOTES Journal article published in Applied Optics, Vol. 44, No. 31, November 1, 2005, published by the Optical Society of America. © 2005 Optical Society of America. The U.S. Government is joint author of the work and has the right to use, modify, reproduce, release, perform, display, or disclose the work. PAO Case Number: AFRL/WS 05-0572; Date cleared: 08 Mar 2005.															
14. ABSTRACT Tunable diode laser absorption measurements of gas temperature and water concentration were made at the exit of a model scramjet combustor fueled on JP-7. Multiplexed, fiber-coupled, near-infrared distributed feedback lasers were used to probe three water vapor absorption features in the 1.34 to 1.47 μm spectral region ($2\nu_1$ and $\nu_1 + \nu_3$ overtone bands). Ratio thermometry was performed using direct absorption wavelength scans of isolated features at a 4-kHz repetition rate, as well as $2f$ wavelength modulation scans at a 2-kHz scan rate. Large signal-to-noise ratios demonstrate the ability of the optimally engineered optical hardware to reject beam steering and vibration noise. Successful measurements were made at full combustion conditions for a variety of fuel/air equivalence ratios and at eight vertical positions in the duct to investigate spatial uniformity. The use of three water vapor absorption features allowed for preliminary estimates of temperature distributions along the line of sight. The improved signal quality afforded by $2f$ measurements, in the case of weak absorption, demonstrates the utility of a scanned wavelength modulation strategy.															
15. SUBJECT TERMS Supersonic combustion, diode laser diagnostic															
16. SECURITY CLASSIFICATION OF:			17. LIMITATION OF ABSTRACT: SAR	18. NUMBER OF PAGES 18	19a. NAME OF RESPONSIBLE PERSON (Monitor) Mark R. Gruber 19b. TELEPHONE NUMBER (Include Area Code) N/A										
a. REPORT Unclassified	b. ABSTRACT Unclassified	c. THIS PAGE Unclassified													

Near-infrared diode laser absorption diagnostic for temperature and water vapor in a scramjet combustor

Jonathan T. C. Liu, Gregory B. Rieker, Jay B. Jeffries, Mark R. Gruber, Campbell D. Carter, Tarun Mathur, and Ronald K. Hanson

Tunable diode laser absorption measurements of gas temperature and water concentration were made at the exit of a model scramjet combustor fueled on JP-7. Multiplexed, fiber-coupled, near-infrared distributed feedback lasers were used to probe three water vapor absorption features in the 1.34–1.47 μm spectral region ($2\nu_1$ and $\nu_1 + \nu_3$ overtone bands). Ratio thermometry was performed using direct-absorption wavelength scans of isolated features at a 4-kHz repetition rate, as well as $2f$ wavelength modulation scans at a 2-kHz scan rate. Large signal-to-noise ratios demonstrate the ability of the optimally engineered optical hardware to reject beam steering and vibration noise. Successful measurements were made at full combustion conditions for a variety of fuel/air equivalence ratios and at eight vertical positions in the duct to investigate spatial uniformity. The use of three water vapor absorption features allowed for preliminary estimates of temperature distributions along the line of sight. The improved signal quality afforded by $2f$ measurements, in the case of weak absorption, demonstrates the utility of a scanned wavelength modulation strategy in such situations. © 2005 Optical Society of America

OCIS codes: 120.0120, 120.1740, 300.0300, 300.1030, 300.6260, 300.6380.

1. Introduction

The history of scramjet engine research spans more than half a century and continues to generate interest as an enabling technology for air-breathing hypersonic propulsion. Although the basic concept of a scramjet engine is straightforward, research in this field has been hampered by a number of challenges. Coupled interactions between shocks and boundary layers exist within the engine, such that complicated engine geometries are required for robust flame holding and heat release. A recent review of scramjet engine development outlines some of these issues.¹

Because of the many challenges and unknowns in

scramjet engine development, diagnostic tools are invaluable for expediting the design and testing process. For any combustion device, gas temperature is paramount for diagnosing combustion efficiency. Water vapor is a major combustion product that is also a key indicator of the extent of combustion. This paper describes a diode laser absorption sensor that interrogates multiple water vapor transitions in the near-infrared spectral region. From the ratio of the measured line strengths of individual spectral features, path-integrated temperatures may be inferred, along with water vapor concentrations in the post-combustion region of a scramjet test facility located at Wright-Patterson Air Force Base (WPAFB) in Ohio.

Diode laser sensors have been gaining popularity in a wide array of practical measurement applications ranging from trace-gas detection^{2–4} and combustion diagnostics^{5–13} to numerous biomedical applications. Their low cost, small size, and simple turn-key operation enable the development of optical sensors that are feasible for a wide range of potential applications. Fiber-coupled diode lasers are especially convenient to route laser radiation in and around test facilities. For probing water vapor features, telecommunications distributed feedback (DFB) lasers exist in the 1.3 to 1.5- μm region, pro-

J. Liu (jonliu@stanfordalumni.org), G. B. Rieker, J. B. Jeffries, and R. K. Hanson are with the High Temperature Gasdynamics Laboratory, Department of Mechanical Engineering, Stanford University, Stanford, California 94305. M. R. Gruber and C. D. Carter are with the Air Force Research Laboratory, Propulsion Sciences and Advanced Concepts Division, Wright-Patterson Air Force Base, Dayton, Ohio 45433. T. Mathur is with Innovative Scientific Solutions, Inc., Dayton, Ohio 45440.

Received 8 February 2005; revised manuscript received 27 April 2005; accepted 17 May 2005.

0003-6935/05/316701-11\$15.00/0

© 2005 Optical Society of America

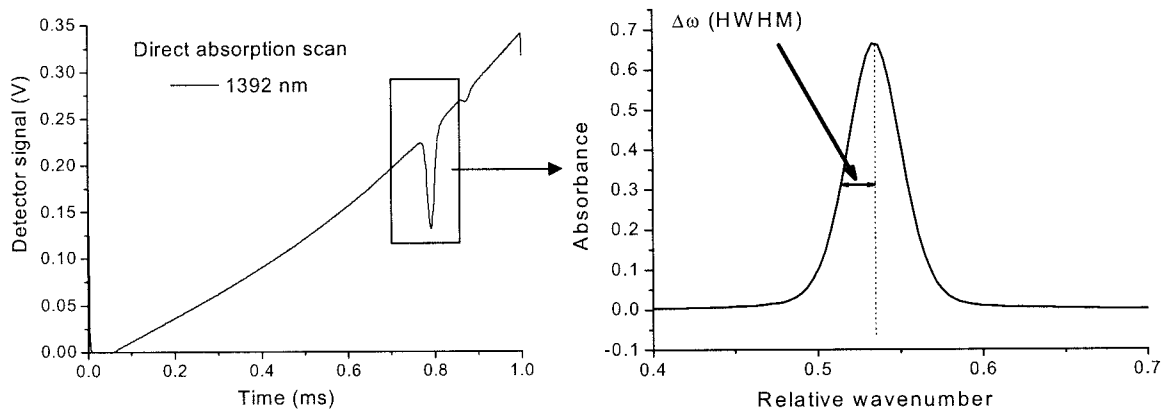


Fig. 1. Left, detected signal for a direct-absorption scan (one scan) near 1392 nm. (b) Right, a typical absorbance plot for an isolated absorption feature.

viding access to water vapor overtone and combination bands ($2\nu_1$ and $\nu_1 + \nu_3$). These DFB lasers are narrowband, single mode, and relatively powerful (10–30 mW) and may be tuned over several wavenumbers at kilohertz rates by modulating the injection current. Static pressures in the postcombustion measurement location in a scramjet engine are on the order of 1 atm, where the linewidths of water absorption features are of order 0.1 cm^{-1} . Therefore, wavelength scans across absorption features at kilohertz rates can be easily accomplished with the DFB lasers used in this study.

Many challenges complicate the implementation of laser-based sensors in realistic engine facilities and are dealt with in this work:

1. The turbulent flow fields of many combustors, such as the scramjet, in which large boundary layers and shock structures exist, lead to variable density gradients within the flow that cause beam steering of probe lasers. Mechanical vibrations may cause additional deviations in laser beam paths. However, the optical hardware can be designed to reject such noise sources and enable the acquisition of data of high signal-to-noise ratio (SNR), as described in Subsection 3.A and demonstrated in Subsection 4.A.

2. Limited optical access and difficult mounting environments make fiber-optic transport of laser radiation extremely valuable. Single-mode fibers are favored for laser beam transmission, as a spatially smooth Gaussian output is desired. However, multimode fibers are favored for light collection in order to provide a larger target for the collection of light in the presence of various beam-steering and misalignment mechanisms. Unfortunately, the light beam exiting a multimode fiber exhibits mode noise, but this can be effectively suppressed by eliminating any losses after the transmitted probe beam is collected (see Subsection 3.A).

3. Temperature and concentration gradients due, for example, to boundary layers, can complicate the interpretation of line-of-sight absorption ratios for gas temperatures. The use of multiple lines provides additional information about the uniformity of tem-

perature distributions along the line of sight, as will be discussed in Subsection 4.C.

4. The SNR in scanned direct absorption measurements is often limited by errors associated with the baseline fitting of absorption features. Derivative techniques like $2f$ spectroscopy offer benefits in cases of weak absorption,¹⁴ as described in Subsection 4.D.

The proof of principle of this sensor is shown in Subsection 4.B, where example results are shown of temperature and water concentration time histories for various combustor conditions and combustor locations. The good temporal resolution of these measurements allows for the frequency power spectrum analysis of the stability of the gas flow.

2. Measurement Principles

A. Direct Absorption Methods

Scanned-wavelength, direct-absorption sensors are useful in measurement applications in which isolated and narrow spectral features exist. A linear variation in injection current is used to scan DFB diode lasers simultaneously in intensity and wavelength. Figure 1(a) shows a typical direct-absorption scan using a diode laser, in which the laser intensity changes in response to an injection current ramp. A polynomial fit to the nonabsorbing wings of the absorption feature is used to extrapolate a zero-absorption baseline, from which an absorbance plot of the absorption feature may be constructed, as shown in Fig. 1.

The fundamental equation for absorption spectroscopy is the Beer–Lambert Law. The Beer–Lambert relation gives the transmitted intensity, I_t , of monochromatic radiation after passing through an absorbing gas, given here for a uniform gas medium,

$$\tau(\nu) = \left(\frac{I_t}{I_0} \right)_\nu = \exp[-\alpha(\nu)L], \quad (1)$$

where $\tau(\nu)$ is the transmission coefficient, I_0 is the incident radiation intensity, $\alpha(\nu)$ is the absorption coefficient, L is the optical absorption path length,

and absorbance is defined as the quantity $\alpha(\nu)L$. The absorption coefficient is the product of line strength, $S[\text{cm}^{-2}/\text{atm}]$, absorbing species partial pressure, $p_i[\text{atm}]$, and line-shape function $\phi(\nu)[\text{cm}]$: $\alpha(\nu) = S\phi(\nu)p_i$. The absorption coefficient is a function of temperature, pressure, and gas composition, which enables these parameters to be inferred through carefully designed spectroscopic measurements.

The line strength of an absorption feature is a function of temperature; the transition frequency, ν_0 ; the lower-state energy of the quantum transition, E'' as well as the partition function of the species, $Q(T)$ (rovibrational states are relevant for near-infrared water vapor spectra):

$$S(T) = S(T_0) \frac{T_0}{T} \frac{Q(T_0)}{Q(T)} \frac{1 - \exp\left(-\frac{h\nu_0}{KT}\right)}{1 - \exp\left(-\frac{h\nu_0}{KT_0}\right)} \times \exp\left[-\frac{hc}{K} E'' \left(\frac{1}{T} - \frac{1}{T_0}\right)\right]. \quad (2)$$

Here, K is Boltzmann's constant, $S(T_0)$ is the line strength at a reference temperature T_0 (generally tabulated at room temperature, 296 K), h is Planck's constant, and c is the speed of light. The partition function has been analytically determined by various researchers who have provided correlations used in our spectral simulations.^{15,16} For water vapor transitions, the HITRAN database^{17,18} provides a compilation of spectroscopic parameters such as line strength and broadening coefficients. However, in our experience, an accurate temperature measurement requires the validation of the HITRAN parameters for selected transitions.¹⁹

In practical measurements, the spectrally integrated absorbance (area) of a transition is often measured, which is directly proportional to line strength:

$$\text{area} = \int_{-\infty}^{\infty} -\ln\left(\frac{I}{I_0}\right) d\nu = S(T)p_{\text{species}}L. \quad (3)$$

The ratio of the integrated absorbance of two transitions is only a function of temperature for multiplexed laser beams probing identical paths:

$$\frac{\text{area}_1}{\text{area}_2} = \frac{S_1(T)}{S_2(T)}. \quad (4)$$

By measuring the integrated absorbance of two transitions, temperature is inferred with Eq. (4), and species concentration is inferred with Eq. (3).

B. 2f Methods

Wavelength modulation spectroscopy (WMS) with 2f detection is a common technique used to improve SNR in measurements as it shifts the detection band to higher frequencies, is phase sensitive, and pro-

vides a zero baseline sensing strategy. However, the improved SNR comes at the expense of additional requirements for calibration. The scramjet engine is well suited for utilizing scanned-2f ratio thermometry because static pressures are relatively low and absorption features are consequently narrow and isolated. The theory of WMS will not be described in detail here, as it is well documented in the literature,^{20–28} along with various practical implementations of WMS for gas sensing using diode lasers.^{29–35}

Since the scramjet facility investigated in our research provided a long measurement path length (23 cm), near-atmospheric pressures, large water vapor mole fractions ($\sim 10\%$), and moderate temperatures (< 2000 K), absorption strengths were generally large enough that direct-absorption methods were ideal. Although direct-absorption methods are preferred for the two strongest lines used in this study, analysis of the weakest line demonstrates the utility of 2f methods for improving SNR for low-absorbance measurements.

3. Experimental

A. Optical Hardware

For scanned-wavelength temperature and concentration sensors, fiber-coupled, DFB diode lasers from NEL America Inc. are multiplexed using a standard single-mode fiber combiner (1×4) designed for the near infrared. Three of the lasers (1392, 1343, and 1469 nm) are temperature tuned to lase at wavelengths near selected absorption features. An external modulation, consisting of either a 4-kHz saw tooth ramp, for direct-absorption scans, or a 2-kHz ramp summed with a faster 190-kHz sinusoidal modulation, for scanned-2f spectroscopy, is fed into each of the current-source units. A fourth laser is a nonresonant laser near 1315 nm that is used to monitor transmission fluctuations.

Fiber optics are useful for routing laser radiation with minimal intrusion such that transmission and collection optics may be easily mounted on the engine test stand. A nonfibered approach using free-space optics is not feasible for most realistic engine diagnostic applications. The fiber-coupled (9- μm single-mode fiber) multiplexed beam is transmitted across a test region using an aspheric collimator (Thorlabs F230FC-C). On the collection side, a larger collimator (Oz Optics HPUCO-25-1300-M-10BQ) is used to focus the free-space beam into a 400- μm diameter multi-mode fiber with a numerical aperture (NA) of 0.39 (Thorlabs M20L05). The 1-cm diameter, 1-cm focal length, Oz Optics collection lens offers a large "sweet spot" for the collection of the collimated laser beam, such that the collection is tolerant of relatively large changes in lateral and angular alignment. This is a key component for minimizing beam-steering-induced laser intensity fluctuations by the turbulent flow field within the combustor. A 400- μm fiber routes the collected signal into a grating-based demultiplexing setup, where a large aspheric lens (Op-

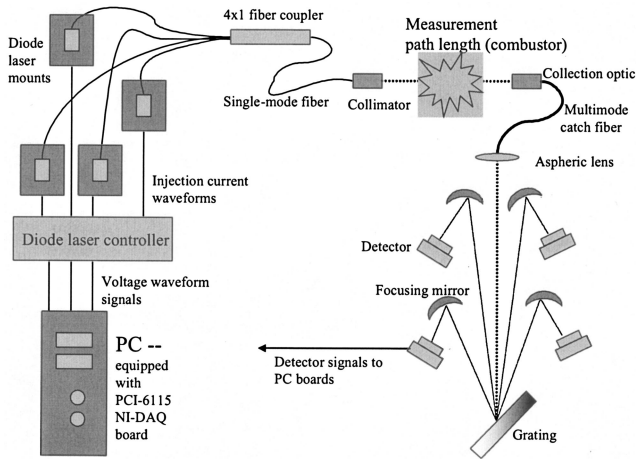


Fig. 2. Optical configuration for two multiplexed lasers. The actual sensor used in these measurements contained four multiplexed lasers.

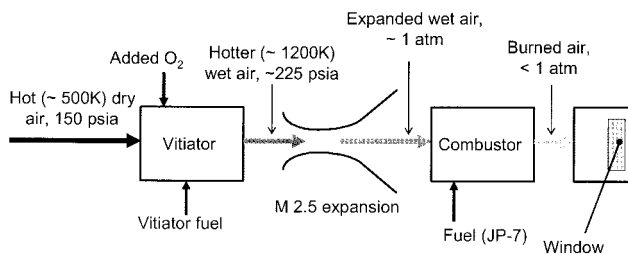


Fig. 3. Block diagram of the SCRAMJET facility.

tosigma 023-2392) is used to collimate the output from the 400- μm fiber and send it onto a 30-mm square diffraction grating (first order) with 1200 grooves/mm (Edmund Optics NT43-852). The demultiplexed beams are then dispersed in space and focused with concave mirrors onto individual 4-MHz large-area (3-mm diameter) amplified InGaAs photodetectors from Electro-Optical Systems Inc. (IGA-030-E5/4MHz).

A benefit of a grating-based dispersion system is that it allows for the rejection of broadband emission

from a combustor. The dispersion system behaves approximately as a 10-nm bandpass filter to reject any flame luminosity captured by the collection fiber. The entire dispersion apparatus is enclosed in a tent and purged with a nitrogen flow to remove ambient water vapor from the dispersion beam paths. Figure 2 illustrates the experimental configuration.

The high-bandwidth large-area detectors insure collection of the entire demultiplexed beam, which minimizes fiber mode noise introduced by the 400- μm collection fiber. Mode noise results from the speckled structure of light emitted from multimode fibers owing to interference between rays of light traveling in different cavity modes within the fiber. Since this structure is wavelength dependent, it can lead to intensity distortions in diode laser wavelength scans if only a portion of the light emitted from a multimode fiber is detected.

Detector signals from all channels are simultaneously recorded at a 4-MHz sampling rate by a National Instruments data-acquisition system using a LabVIEW scope program. The $2f$ line shapes are recovered by running a digital lock-in program on LabVIEW with a low-pass filter time constant of 70 kHz.

B. Scramjet Facility

A detailed description of the scramjet facility at WPAFB will not be presented here. A more complete account of the facility may be found in the literature.³⁶⁻³⁹ A block diagram and schematic of the scramjet facility at WPAFB is shown in Figs. 3 and 4, respectively. An electrically heated dry compressed-air flow is continuously supplied to the direct-connect combustion facility at 13.6 kg/s, up to 5.2 MPa and 920 K total pressure and temperature. The flow is further heated by combustion in a vitiator, which results in a high-temperature (up to 2500 K) and high-pressure flow. Oxygen is added to replenish that which was burned in the vitiator. The hot, high-pressure flow is then expanded to supersonic speeds where it enters a model scramjet combustor. The JP-7 fuel is added and burned in a

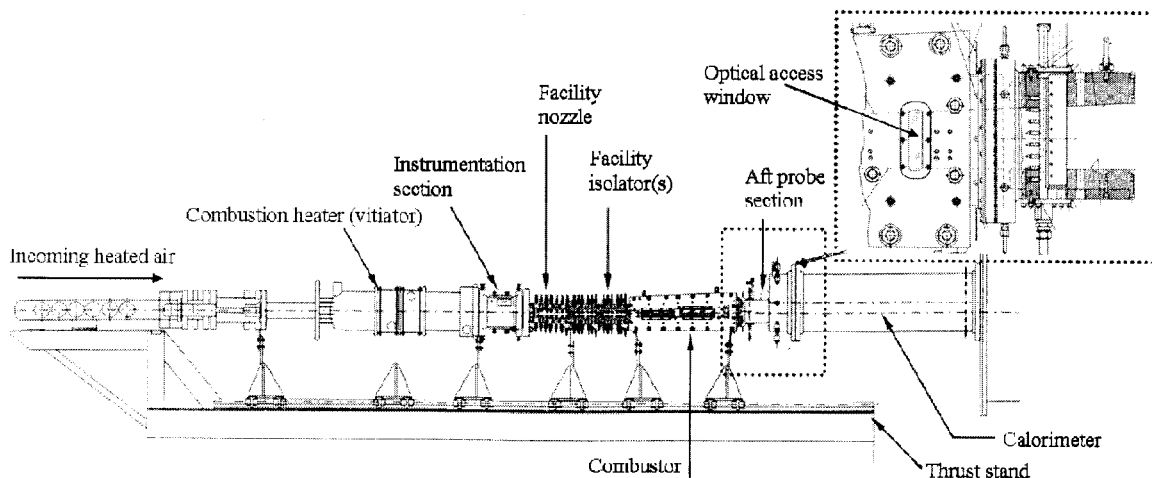


Fig. 4. Schematic of the SCRAMJET facility.

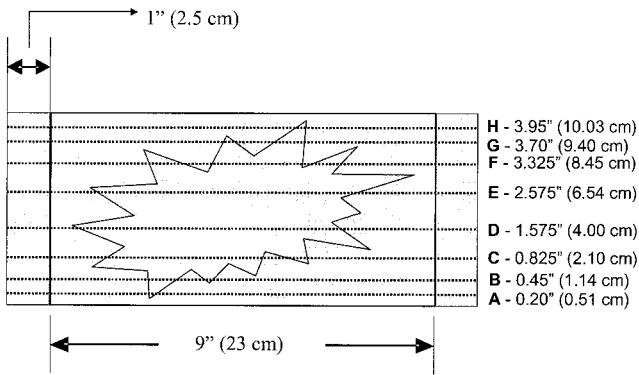


Fig. 5. Location of eight measurement beam paths through the optical access windows (vertical positions A through H).

cavity-based flame holder. Engine runs for the measurements described in this work were of several seconds in duration.

The postcombustion gases are monitored downstream via a rectangular 2.5 cm × 12 cm quartz window. Collimation optics for the transmission and collection of laser radiation were offset from the combustor windows by at least 6 in. to avoid damage due to radiation from flame luminosity. Nitrogen purge tubes were installed to eliminate atmospheric water interference in the sensor's free-space laser paths. Measurements were made along one of eight horizontal spanwise beam paths positioned vertically along the rectangular optical access region, as shown in Fig. 5. Transmission and collection optics were mounted on vertical translation stages on either side of the combustor, so that beam paths could be moved between combustor runs. The precision of the translation stages was sufficient to maintain alignment at all measurement locations.

C. Line Selection and Validation

Spectral features must be selected possessing a combination of lower-state energies such that the ratio of recorded signal strengths is a sensitive function of temperature. Accurate determination of absorption baselines requires isolated spectral features. A discussion of the strategy behind this optimal selection procedure may be found in the literature.^{5,40,41}

The spectral features used in this sensor are tabulated in Table 1. Lower-state energies, E'' , are given by HITRAN04.^{17,18} Line strengths are tabulated from HITRAN04, as well as from our own laboratory val-

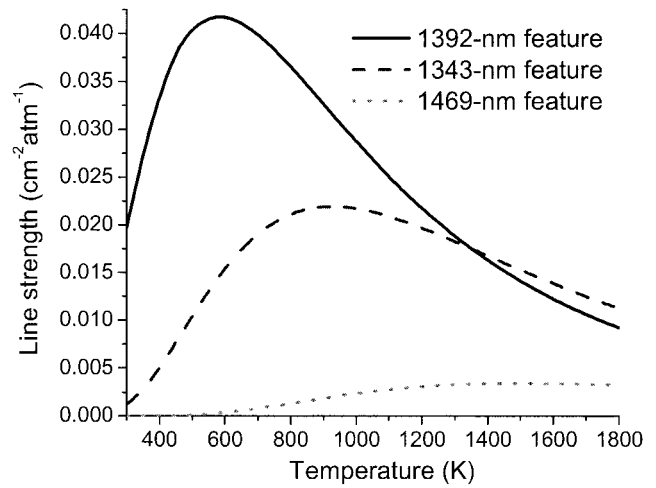


Fig. 6. Line strength versus temperature for water features at 1392, 1343, and 1469 nm, using validated parameters (see Table 1).

idations.^{7,11} A plot of the line strength versus temperature for the three water features used in this study, with laboratory-validated parameters, is shown in Fig. 6.

4. Results

A. Improvements to Signal-to-Noise Ratio

The water vapor absorption data collected here has significantly improved SNR compared with earlier measurements⁴² because of improved optical engineering. Collection optics had a large sweet spot for capturing the collimated laser beam, resulting in excellent tolerance to beam steering. Figure 7 shows a comparison between the single-scan transmission signals reported here (left) and the signals from a previous measurement campaign (right).⁴² The current SNR is approximately 35 times larger than in previous data. The scan rates of the current measurements [Fig. 7, right] are also four times faster (4 kHz) than the scan rates utilized in the earlier measurements [Fig. 7, left]. The most important changes are the use of a larger-diameter collection lens (1 cm), a larger-diameter collection fiber (400- μ m versus 50- μ m), and a collection fiber with a larger NA (0.39 versus 0.22).

Table 1. Line Strength and Lower-State Energy Parameters for Water Vapor Features Used in Measurement Campaigns

Wavelength (nm) HITRAN04	Wavenumber (cm^{-1}) HITRAN04	Line Strength, ^a S ($\text{cm}^{-2} \text{atm}^{-1}$) HITRAN04	Line Strength, ^a S ($\text{cm}^{-2} \text{atm}^{-1}$) Measured	Lower-State Energy (cm^{-1}) HITRAN04
1392	7185.60	$1.97 (10)^{-2}$	$1.96 (10)^{-2}$	1045.1
1343	7444.35+	$1.12 (10)^{-3}$	$1.10 (10)^{-3}$	1774.8
	7444.37 (combined)			1806.7
1469	6807.83	$1.02 (10)^{-6}$	$6.48 (10)^{-7}$	3319.4

^a296 K.

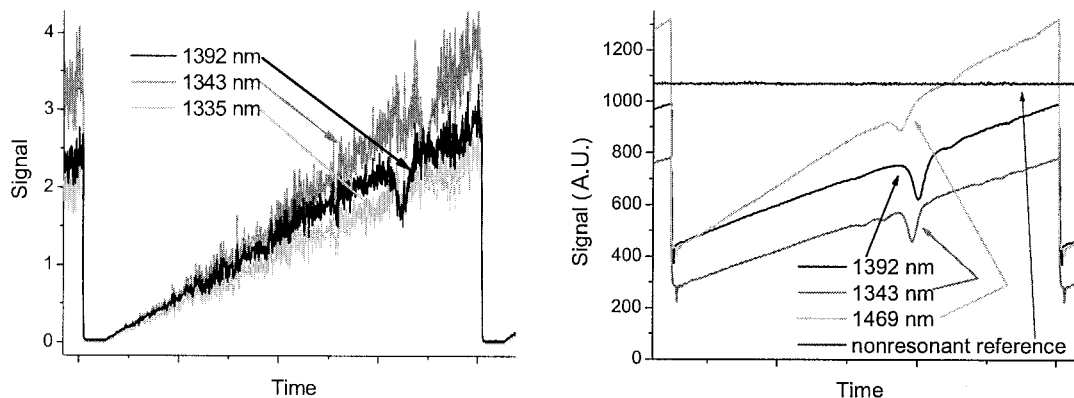


Fig. 7. Left, single multiplexed absorption scan taken at 1 kHz (1-ms scan). Data taken 9/2002. Right, single multiplexed absorption scan taken at 4 kHz (0.25-ms scan). Data taken September 2004.

B. Engine Diagnostics

Temperature and water concentration time histories, at a 4-kHz bandwidth, were acquired to characterize the vitiator, as well as for full combustion runs in the scramjet facility. An example plot of measured temperature and water partial pressure in a vitiator-only flow is shown in Fig. 8. The measurement beam path was at position C (see Fig. 5), and the average static pressure at the window, measured with pressure taps, was 0.22 ± 0.01 atm. Water vapor features at 1392 and 1343 nm were used to infer temperature, as they are relatively strong at these temperatures and exhibit good temperature sensitivity. Temperatures were also inferred by performing Voigt fits to the absorption features and using absorbance area (spectrally integrated absorbance) ratios, which removes the need to know total pressure or gas composition. Absorption peak-height ratios were also used to infer temperatures, utilizing the spectroscopic parameters listed in HITRAN04. Both the peak-height ratio and the area ratio data-analysis methods yield similar temperature results for the vitiator-only measurements. Water partial pressure measurements

may be inferred from temperature measurements and the integrated absorbance of the Voigt-fitted water features.

For full-combustion runs, Voigt-fitted area ratios are used to infer temperature. An example of a temperature and water partial pressure time history measurement is shown in Fig. 9. These measurements utilize the absorption features at 1392 and 1343 nm. A 1-kHz filter is used to smooth the data recorded at a 4-kHz bandwidth.

Temperature and water partial pressure measurements were made across a fixed beam path at position C (see Fig. 5), as a function of combustor fuel/air equivalence ratio. Average results are plotted in Fig. 10, demonstrating the ability of the sensor to capture varying engine conditions, through changes in both temperature and water concentration. Expected temperatures and water concentrations, based on a 1D combustion model, are shown for comparison. These simulations are calculated by scramjet researchers at WPAFB, utilizing information from various engine sensors, such as pressure taps and flow rate moni-

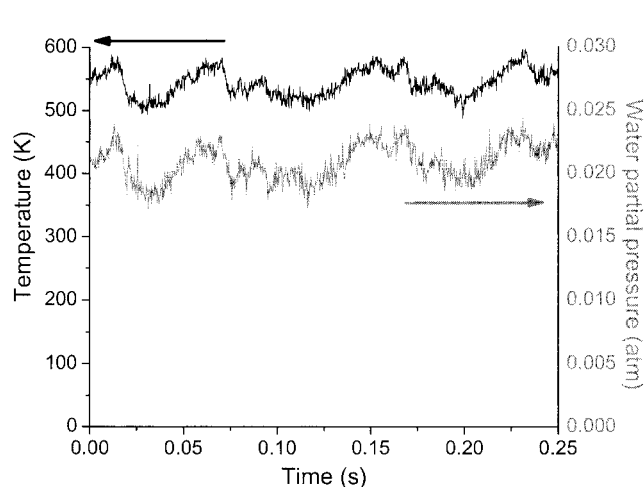


Fig. 8. Vitiator only: Temperature versus time (left axis) and water partial pressure versus time (right axis); 4-kHz bandwidth; position C.

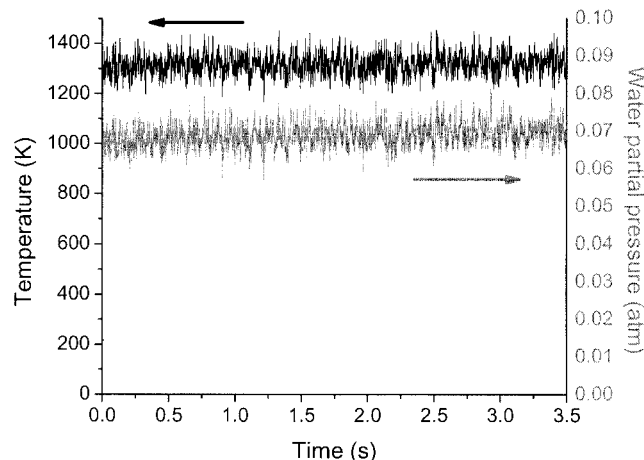


Fig. 9. Full combustion run: Temperature versus time (left axis) and water partial pressure versus time (right axis). Fuel/air equivalence ratio: $\Phi = 1.02$; position C; 4-kHz measurement bandwidth filtered to 1 kHz in this plot.

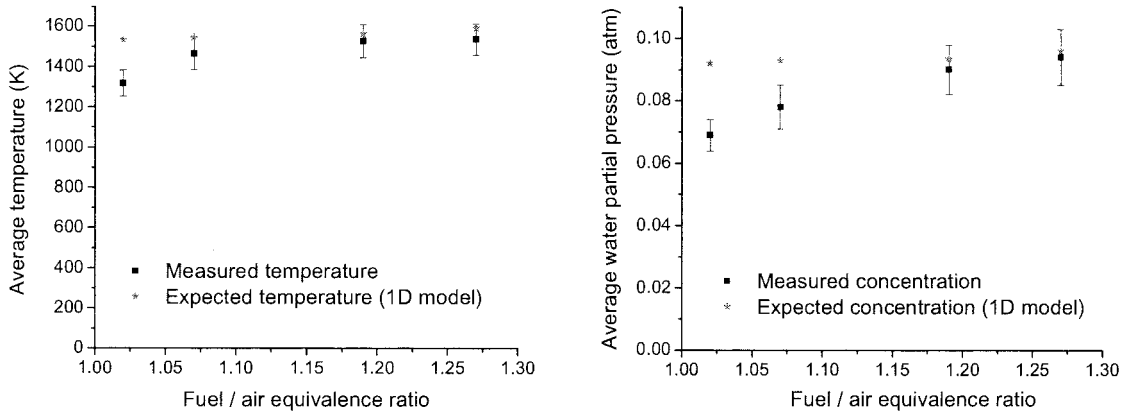


Fig. 10. Left, average temperature versus combustor fuel/air equivalence ratio, Φ . Measured and expected results (based on a combustor 1D model) are shown. The error bars represent a standard deviation in the data at the full 4-kHz bandwidth; position C. Right, average water partial pressure versus combustor fuel/air equivalence ratio, Φ . Measured and expected results (based on a combustor 1D model) are shown. The error bars represent a standard deviation in the data at the full 4-kHz bandwidth; position C.

tors. There is a slight discrepancy between measured and expected results at the lower equivalence ratios, which should be a subject for further investigation. Temperature and water concentrations were also measured across the scramjet combustor at the eight vertical locations shown in Fig. 5. Examples are shown in Fig. 11 with error bars to indicate measurement uncertainty (one standard deviation at the full 4-kHz bandwidth). The presence of larger density gradients at the top of the combustor causes signal quality to degrade because of beam-steering noise, especially at the upper two measurement locations.

The 4-kHz measurement bandwidth of the direct-absorption temperature measurements allows for an analysis of frequency content of up to 2 kHz. A fast fourier transform (FFT) power spectrum of the data shown in Fig. 9 indicates low-frequency modes below 150 Hz, suggesting mechanical vibration frequencies or combustion instabilities. An example power spectrum is shown in Fig. 12, where distinct frequency modes are noticeable at ~ 21 , ~ 63 , and ~ 116 Hz.

Such frequency content is of value to engine designers who desire to suppress such fluctuations by mechanical design and/or active combustion control. These results illustrate the value of time-resolved temperature measurements for aerospace ground test experiments.

C. Line-of-Sight Temperature Distribution

The scramjet combustor, as with nearly all practical combustors, does not exhibit a uniform temperature profile across the measurement path. The vertically scanned temperature measurements shown in Fig. 11 indicate large spatial variations, which certainly exist along the measurement paths as well. Numerous researchers have attempted to make corrections for boundary layer effects.^{40,41,43,44} However, these techniques are limited and require prior knowledge of the general shape of the spatial temperature profile to be effective. The problem of solving for a temperature distribution along a line of sight by probing

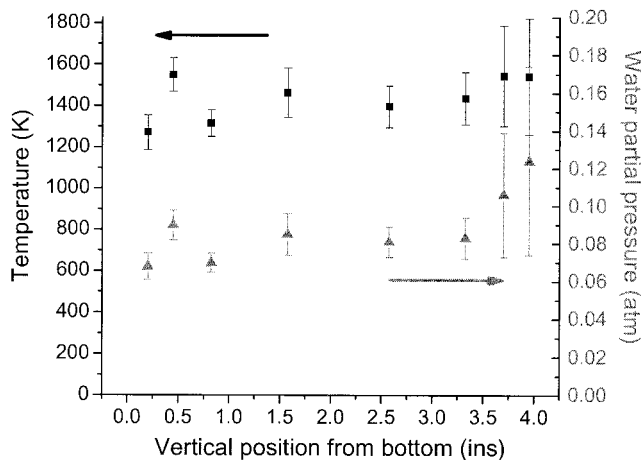


Fig. 11. Time-averaged temperature (left axis) and water partial pressure (right axis) versus vertical measurement path location. Fuel/air equivalence ratio: $\Phi \sim 1.00$; 4-kHz; bandwidth.

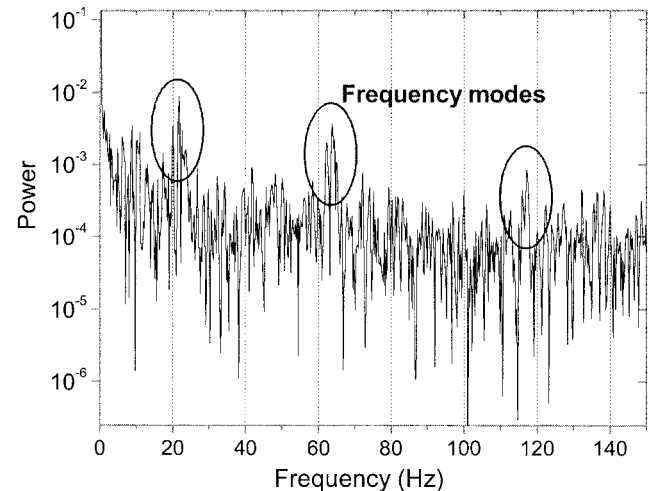


Fig. 12. FFT power spectrum (0–150 Hz shown) of the temperature versus time data plotted in Fig. 10. Fuel/air equivalence ratio: $\Phi = 1.02$; position C.

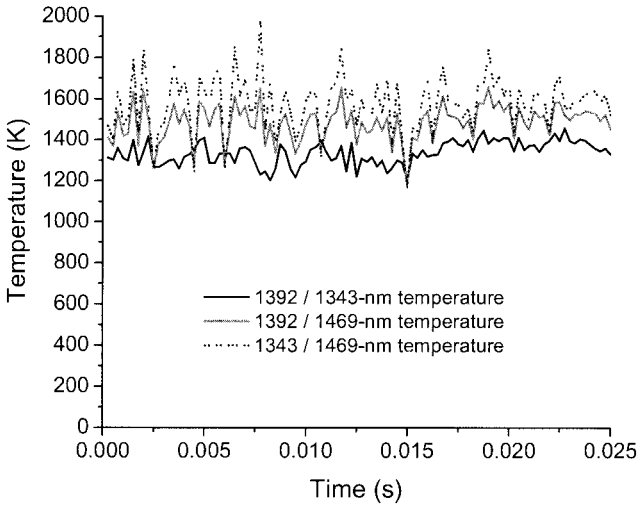


Fig. 13. Temperatures calculated assuming a uniform path and using various area ratio combinations. Fuel/air equivalence ratio: $\Phi = 1.02$; position C.

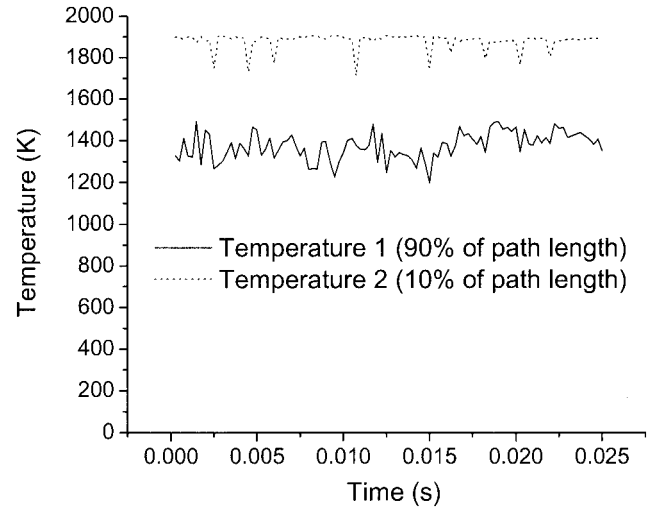


Fig. 14. Numerical solution assuming two temperature bins (T_1 and T_2) of size 90% and 10% of the total path length and a uniform water concentration. Fuel/air equivalence ratio: $\Phi = 1.02$; position C.

multiple absorption features may be described with a matrix equation⁴⁴:

$$\begin{bmatrix} S_1(T_1) & S_1(T_2) & S_1(T_n) \\ S_2(T_1) & S_2(T_2) & S_2(T_n) \\ S_m(T_1) & S_2(T_2) & S_m(T_n) \end{bmatrix} \begin{bmatrix} p_1 L_1 \\ p_2 L_2 \\ p_n L_n \end{bmatrix} = \begin{bmatrix} \text{area}_1 \\ \text{area}_2 \\ \text{area}_m \end{bmatrix}. \quad (5)$$

Two area measurements allow for the solution of two measurement parameters, T_1 and $p_1 L_1$, where L_1 is known in this case (total path length):

$$\begin{bmatrix} S_1(T_1) \\ S_2(T_1) \end{bmatrix} p_1 L_1 = \begin{bmatrix} \text{area}_1 \\ \text{area}_2 \end{bmatrix}. \quad (6)$$

Dividing the first row by the second row in Eq. (6) yields the familiar simplification, used in ratio thermometry, to infer an average temperature with two lines. In this case, the area ratio is equivalent to line strength ratio, as expressed in Eq. (4).

The scramjet sensor utilized in this work provides three integrated absorbance measurements and may be solved to yield three parameters. Assuming that we want to solve for two temperatures, T_1 and T_2 certain parameters must be prescribed to solve for a third parameter amongst the unknowns p_1 , L_1 , p_2 , and L_2 :

$$\begin{bmatrix} S_1(T_1) & S_1(T_2) \\ S_2(T_1) & S_2(T_2) \\ S_3(T_1) & S_3(T_2) \end{bmatrix} \begin{bmatrix} p_1 L_1 \\ p_2 L_2 \end{bmatrix} = \begin{bmatrix} \text{area}_1 \\ \text{area}_2 \\ \text{area}_3 \end{bmatrix}. \quad (7)$$

For example, the path lengths of each temperature bin, L_1 and L_2 , may be exactly prescribed and the assumption made that concentration is a constant, $p_1 = p_2$. Therefore, the remaining three terms to be solved are T_1 , T_2 , and $p_1 = p_2 = p$. In reality, for a combustion product like water, species partial pressure is also a function of temperature, as evidenced

by the correlation between these quantities in Figs. 9–12. This situation results in an underdetermined system with four unknowns and three equations. One may use thermodynamic arguments to assume an *a priori* temperature functionality for the partial pressure, $p(T)$, but this results in an overdetermined system with two unknowns (T_1 and T_2) and three equations.

As an initial step, it is useful to assume a uniform temperature distribution along the measurement beam path in the scramjet and infer temperatures using the 1392-nm/1343-nm line pair, the 1392-nm/1469-nm line pair, as well as the 1343-nm/1469-nm line pair. An example result is shown in Fig. 13. The temperatures that are calculated with the 1469-nm line exhibit higher average temperatures and larger scatter than the 1392-nm/1343-nm line pair. The increased scatter is to be expected based on the results shown in Fig. 13, which indicated reduced SNR for the direct-absorption measurements at 1469 nm. It is reasonable to expect that the 1392-nm line yields the lowest temperatures since this low- E'' line is particularly sensitive to lower temperatures. A review of Fig. 6 shows that the line strength of the 1392-nm feature increases greatly at lower temperatures. Compared with the higher- E'' lines, the presence of locally cold regions disproportionately affects the 1392-nm line.

By assuming that the measurement path contains a two-temperature distribution of prescribed lengths (L_1 and L_2), and that the water concentration is constant throughout ($p_1 = p_2 = p$), it is possible to solve the nonlinear system of equations in Eq. (7) for T_1 , T_2 , and p . The data used to create Fig. 13 is solved for these quantities using a Levenberg-Marquardt nonlinear routine, as shown in Fig. 14. The simple model used to solve these equations assumes that 90% of the path length is at one temper-

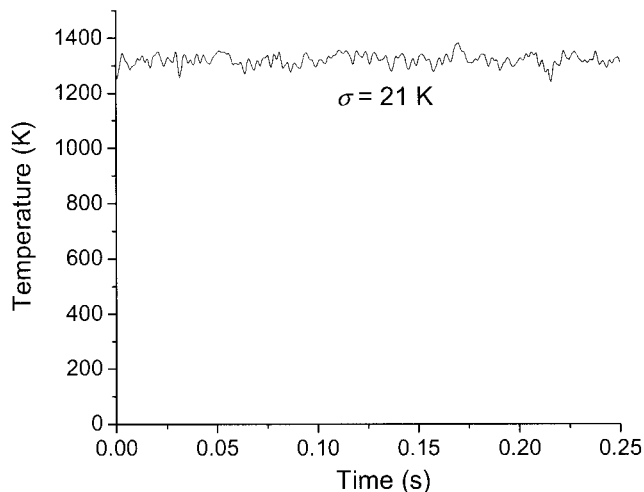


Fig. 15. Temperature versus time using scanned- $2f$ wavelength modulation spectroscopy. The $2f$ peak ratios of water features at 1392 and 1469 nm are used. Fuel/air equivalence ratio: $\Phi = 1.02$; 1-kHz bandwidth; position C.

ature, T_1 , and that 10% of the path is at T_2 . This would reflect, for example, the presence of a hot boundary layer next to the combustor side walls. Numerical fluid simulations of the scramjet combustor predict that the fuel from the cavity-based injectors tends to migrate toward the side walls of the duct. This would lead to greater heat release at the walls, resulting in higher temperatures, as indicated by this idealized interpretation of the absorption data. In addition, deceleration of the flow in the side-wall boundary layer would cause kinetic energy to be converted into increased thermal energy (and thus higher temperatures). By probing only three water features, it is difficult to perform a realistic analysis of line-of-sight distributions. Although the solution used for Fig. 14 is numerically efficient, given the few data points available, an accurate result clearly would require the use of additional lines. These lines should be selected to provide good SNR as well as sensitivity to the nonuniform temperature field. Addressing these issues is the subject of future work. Nonetheless, the current data set provides some indication of higher temperatures near the walls, as well as serves to illustrate the potential of multiwavelength absorption techniques.

D. $2f$ Spectroscopy

Although the large absorbance levels in this relatively long-path combustor make direct-absorption scans an ideal choice for obtaining temperature and concentration measurements for the strongest water absorption features, a few runs were analyzed using scanned- $2f$ wavelength modulation spectroscopy to verify the benefits of this strategy in the case of weak absorption, as demonstrated by the 1469-nm line. Figure 15 shows a quarter-second of time-resolved $2f$ temperature measurements using the 1392-nm/1469-nm line pair, filtered from a 2-kHz scan rate to a 1-kHz measurement band-

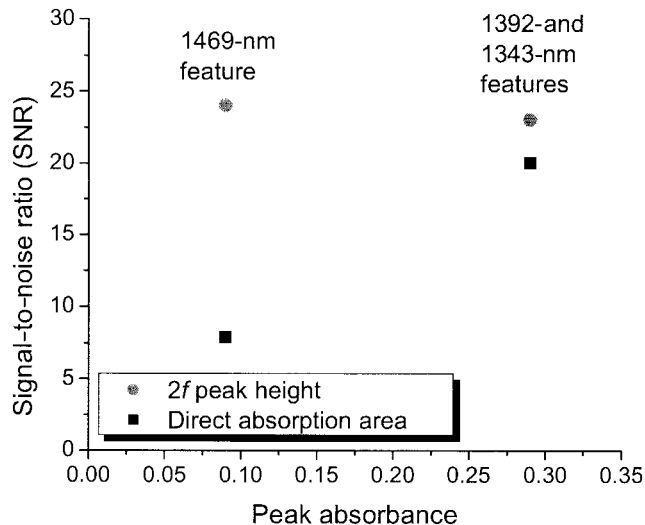


Fig. 16. SNR comparison for direct absorption area and $2f$ peak height measurements as a function of peak absorbance magnitude. Fuel/air equivalence ratio: $\Phi = 1.02$; 1-kHz bandwidth; position C.

width that is analogous to the direct-absorption plot of Fig. 9. The measurement location and the combustor conditions for the measurements shown in Figs. 9 and 15 are identical, and the average temperature measured in Fig. 9 (direct absorption) is used to calibrate the $2f$ measurement. The standard deviation variation in the average temperature in Fig. 15 is 21 K, which is less than the corresponding variation of 40 K with the direct-absorption results shown in Fig. 9.

The true strength of the $2f$ method lies in its ability to significantly improve SNR for weakly absorbing features.^{3,24} As detailed in an earlier work,¹⁴ $2f$ peak height ratios are simply interpreted as being proportional to line strength ratios if modulation depths are optimized AND if absorption levels are low (less than 10% absorption typically). Therefore, the long-path scramjet combustor, in which absorption levels are relatively high for the lines utilized in this study, is not an ideal test bed for ratio thermometry with $2f$ spectroscopy. However, by comparing the SNR of direct-absorption measurements versus $2f$ peak-height measurements, for the strong lines at 1392 and 1343 nm, as well as for the weaker line at 1469-nm, it is apparent that the $2f$ technique is superior for weaker features. Figure 16 shows a comparison of the SNR (spectrally integrated absorbance or $2f$ peak heights as a function of time) of the individual water features for the identical combustion runs shown in Figs. 9 (direct absorption) and 15 ($2f$ spectroscopy). For this combustor condition, the peak absorbance of the 1392 and the 1343-nm feature are comparable (~ 0.3). The SNR of the spectrally integrated absorbance strengths (area under the Voigt curve) of many measurements over time is similar to the SNR of $2f$ peak heights over time (~ 22). For the weaker feature at 1469 nm, the direct-absorption SNR is much degraded, whereas the $2f$ SNR is unchanged (hence, the $2f$ temperature plot in

Fig. 15 utilizes the 1469-nm line). These results provide evidence that in realistic combustion environments, $2f$ methods improve SNR when one is dealing with weak absorption. The high-frequency phase-sensitive detection utilized in modulation spectroscopy helps to reject noise. Additionally, and perhaps more important, the derivative nature of $2f$ spectroscopy eliminates the need to perform baseline fits, which is a large source of uncertainty when one is dealing with weak transitions or broadened spectral features.^{14,45}

The scanned- $2f$ method used here requires calibration and is a relative temperature measurement, whereas direct-absorption scans yield absolute temperature as well as species concentration information. With some additional work, it should be possible to make absolute temperature and concentration measurements with scanned- $2f$ spectroscopy. If experiments are conducted to validate or obtain accurate spectroscopic parameters such as broadening widths, exponents for the temperature dependency of the broadening widths, pressure shift parameters, lower-state energies, and line strengths, it is possible to simulate $2f$ line shapes for arbitrary conditions, provided that the exact wavelength modulation depth and intensity modulation depths are recorded. Since $2f$ signal strengths are proportional to detected laser intensity, $2f$ signals must be normalized by the dc signal strength, or equivalently, in many cases, the $1f$ signal.³⁴ A single calibration measurement, preferably at a condition similar to the measurement conditions, is all that is necessary to establish a scaling factor between $2f$ measurements and $2f$ simulations. This is similar to what is done for large-modulation-depth $2f$ spectroscopy of broad spectral features, as detailed in a previous article.⁴⁴

5. Conclusions

A tunable-diode-laser-based sensor has been developed for line-of-sight temperature and concentration measurements of water vapor in a model scramjet combustor. Both direct absorption scans at 4 kHz and $2f$ wavelength modulation scans at 2 kHz were used to obtain line-shape profiles of three isolated water features near 1392, 1343, and 1469 nm. Integrated direct-absorbance area ratios were used to infer temperature and water vapor concentration at a variety of engine conditions as well as at various vertical path locations across the postcombustion region. Optimized optical components and hardware have yielded excellent signal quality in the probe beams pitched across the supersonic, long-path-length flow field. The use of three multiplexed lasers in the current sensor has allowed for a preliminary discussion of line-of-sight temperature distributions. Results from scanned- $2f$ measurements indicate improved SNR for weakly absorbing transitions, although calibration is necessary for absolute temperature and concentration measurements.

This research was sponsored by the Air Force Office of Scientific Research (AFOSR), Aerospace and

Materials Science Directorate, with Julian Tishkoff as technical monitor.

References

1. E. T. Curran, "Scramjet engines: the first forty years," *J. Propulsion and Power* **17**, 1138–1148 (2001).
2. A. O'Keefe, J. J. Scherer, and J. B. Paul, "CW-integrated cavity output spectroscopy," *Chem. Phys. Lett.* **307**, 343–349 (1999).
3. J. A. Silver and D. J. Kane, "Diode laser measurements of concentration and temperature in microgravity combustion," *Meas. Sci. Technol.* **10**, 845–852 (1999).
4. J. T. C. Liu, R. K. Hanson, and J. B. Jeffries, "High-sensitivity absorption diagnostic for NO₂ using a blue diode laser," *J. Quant. Spectrosc. Radiat. Transfer* **72**, 655–664 (2002).
5. M. P. Arroyo and R. K. Hanson, "Absorption measurements of water-vapor concentration, temperature, and line-shape parameters using a tunable InGaAsP diode laser," *Appl. Opt.* **32**, 6104–6116 (1993).
6. D. S. Baer, V. Nagali, E. R. Furlong, and R. K. Hanson, "Scanned- and fixed-wavelength absorption diagnostics for combustion measurements using multiplexed diode lasers," *AIAA J.* **34**, 489–793 (1996).
7. E. R. Furlong, D. S. Baer, and R. K. Hanson, "Combustion control and monitoring using a multiplexed diode-laser sensor system," *Proc. Combust. Inst.* **26**, 2851–2858 (1996).
8. M. G. Allen, "Diode laser absorption sensors for gas-dynamic and combustion flows," *Meas. Sci. Technol.* **9**, 545–562 (1998).
9. V. Ebert, T. Fernholz, C. Giesemann, H. Pitz, H. Teichert, J. Wolfrum, and H. Jaritz, "A NIR-diode laser spectrometer with closed-loop alignment control for simultaneous *in-situ* detection of multiple species and temperature in a gas-fired power-plant for active combustion control purposes," *Proc. Combust. Inst.* **28**, 423–430 (2000).
10. D. Richter, D. G. Lancaster, and F. K. Tittel, "Development of an automated diode laser based multicomponent gas sensor," *Appl. Opt.* **39**, 4444–4450 (2000).
11. S. T. Sanders, J. A. Baldwin, T. P. Jenkins, D. S. Baer, and R. K. Hanson, "Diode-laser sensor for monitoring multiple combustion parameters in pulse detonation engines," *Proce. Combust. Inst.* **28**, 587–594 (2000).
12. M. A. Allen, E. R. Furlong, and R. K. Hanson, "Tunable diode laser sensing and combustion control," in *Applied Combustion Diagnostics*, K. Kohse-Hoinghaus and J. B. Jeffries, eds. (Taylor and Francis, 2002), pp. 479–498.
13. H. Teichert, T. Fernholtz, and V. Ebert, "Simultaneous *in situ* measurement of CO, H₂O, and gas temperatures in a full-sized coal-fired power plant by near-infrared diode lasers," *Appl. Opt.* **42**, 2043–2051 (2003).
14. J. T. C. Liu, J. B. Jeffries, and R. K. Hanson, "Wavelength modulation absorption spectroscopy with $2f$ detection using multiplexed diode lasers for rapid temperature measurements in gaseous flows," *Appl. Phys. B* **78**, 503–511 (2004).
15. G. J. Harris, S. Viti, H. Y. Mussa, and J. Tennyson, "Calculated high-temperature partition function and related thermodynamic data for H₂O," *J. Chem. Phys.* **9**, 7197–7204 (1998).
16. R. R. Gamache, S. Kennedy, R. Hawkins, and L. S. Rothman, "Total internal partition sums for molecules in the terrestrial atmosphere," *J. Mol. Structure* **517–518**, 407–425 (2000).
17. L. S. Rothman, A. Barbe, D. C. Benner, L. R. Brown, C. Camy-Peyret, M. R. Carleer, K. Chance, C. Clerbaux, V. Dana, V. M. Devi, A. Fayt, J.-M. Flaud, R. R. Gamache, A. Goldman, D. Jacquemart, K. W. Jucks, W. J. Lafferty, J.-Y. Mandin, S. T. Massie, V. Nemtchinov, D. A. Newnham, A. Perrin, C. P. Rinsland, J. Schroeder, K. M. Smith, M. A. H. Smith, K. Tang, R. A. Toth, J. Vander Auwera, P. Varanasi, and K. Yoshino, "The HITRAN molecular spectroscopic database: edition of 2000

- including updates of 2001," *J. Quant. Spectrosc. Radiat. Transfer* **82**, 5–44 (2003).
18. <http://cfa-www.harvard.edu/hitran/>.
 19. X. Liu, X. Zhou, J. B. Jeffries, and R. K. Hanson, "Experimental study of H₂O spectroscopic parameters in the near-IR," paper AIAA-2005-0829, presented at the Forty-Third AIAA Aerospace Sciences Meeting and Exhibit, Reno, Nevada, 10–13 January 2005.
 20. H. Wahlquist, "Modulation broadening of unsaturated lorentzian lines," *J. Chem. Phys.* **35**, 1708–1710 (1961).
 21. G. V. H. Wilson, "Modulation broadening of NMR and ESR line shapes," *J. Appl. Phys.* **34**, 3276–3285 (1963).
 22. R. Arndt, "Analytical line shapes for lorentzian signals broadened by modulation," *J. Appl. Phys.* **36**, 2522–2524 (1965).
 23. J. Reid and D. Labrie, "Second-harmonic detection with tunable diode lasers—comparison experiment and theory," *Appl. Phys. B* **26**, 203–210 (1981).
 24. D. S. Bomse, A. S. Stanton, and J. A. Silver, "Frequency modulation and wavelength modulation spectroscopies: comparison of experimental methods using a lead-salt diode laser," *Appl. Opt.* **31**, 718–731 (1992).
 25. N. Goldstein, S. Adler-Golden, J. Lee, and F. Bien, "Measurement of molecular concentrations and line parameters using line-locked second harmonic spectroscopy with an AlGaAs diode laser," *Appl. Opt.* **31**, 3409–3415 (1992).
 26. J. M. Supplee, E. A. Whittaker, and W. Lenth, "Theoretical description of frequency modulation and wavelength modulation spectroscopy," *Appl. Opt.* **33**, 6294–6302 (1994).
 27. P. Kluczynski and O. Axner, "Theoretical description based on Fourier analysis of wavelength-modulation spectrometry in terms of analytical and background signals," *Appl. Opt.* **38**, 5803–5815 (1999).
 28. S. Schilt, L. Thevenaz, and P. Robert, "Wavelength modulation spectroscopy: combined frequency and intensity laser modulation," *Appl. Opt.* **42**, 6728–6738 (2003).
 29. L. C. Philippe and R. K. Hanson, "Laser diode wavelength-modulation spectroscopy for simultaneous measurement of temperature, pressure, and velocity in shock-heated oxygen flows," *Appl. Opt.* **32**, 6090–6103 (1993).
 30. J. A. Silver and D. J. Kane, "Diode laser measurements of concentration and temperature in microgravity combustion," *Meas. Sci. Technol.* **10**, 845–852 (1999).
 31. T. Aizawa, "Diode-laser wavelength-modulation absorption spectroscopy for quantitative *in situ* measurements of temperature and OH radical concentration in combustion gases," *Appl. Opt.* **40**, 4894–4903 (2001).
 32. S. I. Chou, D. S. Baer, R. K. Hanson, W. Z. Collison, and T. Q. Ni, "HBr concentration and temperature measurements in a plasma etch reactor using diode laser absorption spectroscopy," *J. Vac. Sci. Technol. B* **19**, 477–484 (2001).
 33. D. C. Hovde, J. T. Hodges, G. E. Scace, and J. A. Silver, "Wavelength-modulation laser hydrometer for ultrasensitive detection of water vapor in semiconductor gases," *Appl. Opt.* **40**, 829–839 (2001).
 34. T. Fernholtz, H. Teichert, and V. Ebert, "Digital, phase-sensitive detection for *in situ* diode-laser spectroscopy under rapidly changing transmission conditions," *Appl. Phys. B* **75**, 229–236 (2002).
 35. T. P. Jenkins, P. A. DeBarber, and M. Oljaca, "A rugged low-cost diode laser sensor for H₂O and temperature applied to a spray flame," paper AIAA 2003-0585, presented at the Forty-First Aerospace Sciences Meeting and Exhibit of the American Institute of Aeronautics and Astronautics, Reno, Nevada, 6–9 January 2003.
 36. R. A. Baurle, T. Mathur, M. R. Gruber, and K. R. Jackson, "A numerical and experimental investigation of a scramjet combustor for hypersonic missile applications," AIAA paper 98-3121, presented at the Thirty-Fourth AIAA/ASME/SAE/ASEE Joint Propulsion Conference and Exhibit, Cleveland, Ohio, 13–15 July 1998.
 37. K. Jackson, M. Gruber, T. Mathur, G. Streby, C. Smith, and F. Billig, "Calibration of a newly developed direct-connect high-enthalpy supersonic combustion research facility," AIAA paper 98-1510, presented at the Eighth AIAA International/Space Planes and Hypersonic Systems and Technologies Conference, Norfolk, Virginia, 27–30 April 1998.
 38. T. Mathur, G. Streby, M. Gruber, K. Jackson, J. Donbar, W. Donaldson, T. Jackson, C. Smith, and F. Billig, "Supersonic combustion experiments with a cavity-based fuel injector," AIAA paper 99-2102, presented at the Thirty-Fifth AIAA/ASME/SAE/ASEE Joint Propulsion Conference and Exhibit, Los Angeles, California, 20–24 June 1999.
 39. M. Gruber, K. Jackson, T. Mathur, and F. Billig, "Experiments with a cavity-based fuel injector for scramjet applications," ISABE paper IS-7154, in proceeding of the Twenty-Seventh international Symposium on Air Breathing Engines, September 1999.
 40. X. Ouyang and P. L. Varghese, "Line-of-sight absorption measurements of high temperature gases with thermal and concentration boundary layers," *Appl. Opt.* **28**, 3979–3984 (1989).
 41. X. Zhou, X. Liu, J. B. Jeffries, and R. K. Hanson, "Development of a sensor for temperature and water concentration in combustion gases using a single tunable diode laser," *Meas. Sci. Technol.* **14**, 1459–1468 (2003).
 42. J. T. C. Liu, J. B. Jeffries, R. K. Hanson, S. Creighton, J. A. Lovett, and D. T. Shouse, "Diode laser absorption diagnostics for measurements in practical combustion flow fields," paper AIAA-2003-4581, presented at the Thirty Ninth AIAA/ASME/SAE/ASEE Joint Propulsion Conference, Huntsville, Alabama, 20–23 July 2003.
 43. S. M. Schoenung and R. K. Hanson, "CO and temperature measurements in a flat flame by laser absorption spectroscopy and probe techniques," *Combust. Sci. Technol.* **24**, 227–237 (1981).
 44. S. T. Sanders, J. Wang, J. B. Jeffries, and R. K. Hanson, "Diode-laser absorption sensor for line-of-sight gas temperature distributions," *Appl. Opt.* **40**, 4404–4415 (2001).
 45. J. T. C. Liu, J. B. Jeffries, and R. K. Hanson, "Large-modulation-depth $2f$ spectroscopy with diode lasers for rapid temperature and species measurements in gases with blended and broadened spectra," *Appl. Opt.* **43**, 6500–6509 (2004).